

NEAREST NEIGHBOUR CLASSIFICATION ON LASER POINT CLOUDS TO GAIN OBJECT STRUCTURES FROM BUILDINGS

B. Jutzi^a, H. Gross^b

^a Institute of Photogrammetry and Remote Sensing, Universität Karlsruhe, Englerstr. 7, 76128 Karlsruhe, Germany
boris.jutzi@ipf.uni-karlsruhe.de

^b FGAN-FOM, Research Institute for Optronics and Pattern Recognition, Gutleuthausstraße 1, 76275 Ettlingen, Germany
gross@fom.fgan.de

KEY WORDS: Laser data, point cloud, classification, nearest neighbour, covariance, eigenvalues.

ABSTRACT:

The application of three dimensional building models has become more and more important for urban planning, enhanced navigation and visualization of touristy or historic objects. 3D models can be used to describe complex urban scenes. The automatic generation of 3D models using elevation data is a challenge for actual research. Especially extracting planes edges and corners of man made objects is of great interest. This paper deals with the automatic classification of points by utilizing the eigenvalues of the covariance within the close neighbourhood. The method is based on the analysis of 3D point clouds derived from Laser scanner data. For each 3D point additional structural features by considering the neighbourhood are calculated. Invariance with respect to position, scale and rotation is achieved by normalization of the features. For classification the derived features are compared with analytical calculated as well as trained feature values for typical object structures. For the generation of a training data set several point sets with different density and varying noise are generated and exploited. The result of the investigations is that the quality of the classification using the analytical eigenvalues as reference is not harmful in comparison to the trained data set for a small noise. Therefore for all structures presented here it is not necessary to use training data sets instead of an unsupervised classification based on the analytical eigenvalues. Weighting the calculated distances in the eigenvalue space dependent on the structure type improves the classification result. Due to this classification all points which may belong to a building edge are selected. Assembling these points to lines the 3D borders of the objects were achieved. The algorithm is tested for several urban scenes and the results are discussed.

1. INTRODUCTION

Three-dimensional building models have become important during the past for various applications like urban planning, enhanced navigation or visualization of touristy or historic objects. They can increase the understanding and explanation of complex scenes and support the decision process of operation planning. The benefit for several applications by utilizing LIDAR data was demonstrated for instance by Brenner et al. (2001). For decision support and operation planning the real urban environment should be available. In most cases the object models of interest are not obtainable and especially in time critical situations the 3D models must be generated as fast and accurate as possible.

Different approaches to generate the 3D models of urban scenes are discussed in the literature (Shan & Toth, 2008). Building models are typically acquired by (semi-) automatic processing of Laser scanner elevation data or aerial imagery (Baillard et al., 1999; Geibel & Stilla, 2000). LIDAR data can be utilized for large urban scenes (Gross & Thoennesen, 2005). The processing of raw full-waveform data to gain object structures of buildings was investigated by Jutzi et al. (2005) and the iterative processing to increase the set of 3D points of buildings by Kirchof et al. (2008). Pollefeys (1999) uses projective geometry for a 3D reconstruction from image sequences. Fraser et al. (2002) use stereo approaches for 3D building reconstruction. Vosselman et al. (2004) describes a scan line segmentation method grouping points in a 3D proximity. Airborne systems are widely used but also terrestrial Laser scanners are increasingly available. The latter ones provide a much higher geometrical resolution and accuracy (mm vs. dm) and they are able to acquire fine building facade details which are an essential requirement for a realistic virtual visualization.

In Section 2 the calculation of additional point features is described. The features are normalized with respect to translation, scale and rotation. In Section 3 typical constellations of points are discussed and discriminating features are presented. Examples for the combination of eigenvalues and structure tensor are shown. For typical situations analytical feature values are derived. For the classification procedure the results of the trained feature values are discussed in Section 4 and the trained values are compared with the analytical values. The generation of lines is described in Section 5. Points with the same eigenvectors are assembled and approximated by lines. The resulting 3D structures (boundaries) of objects are shown for the selected laser point cloud. In Section 6 the possibilities using additional features are summarized. Outstanding topics and aspects of the realized method are discussed.

2. EIGENVALUE ESTIMATION TO GAIN OBJECT STRUCTURES

A Laserscanning device delivers 3D point measurements in an Euclidian coordinate system. For airborne systems mostly the height information is stored in a raster grid with a predefined resolution. Image cells without a measurement are interpolated by considering their neighbourhood.

An example data set gathered by an airborne Laser scanner system (TopoSys®) as 3D points is shown in Figure 1a. The color corresponds to the height. A transformation to a raster image, selecting the highest value for each pixel and after filling missing pixels with a Median operation, yields to Figure 1b. Due to the filtering the image does not represent the original 3D information anymore. The horizontal position is slightly different and some of the height values are interpolated to fill the gaps even if there was no measured value available.

Additionally, sometimes more than one measurement for a resolution cell exists considering first and last echo or combining data of several measurement campaigns.

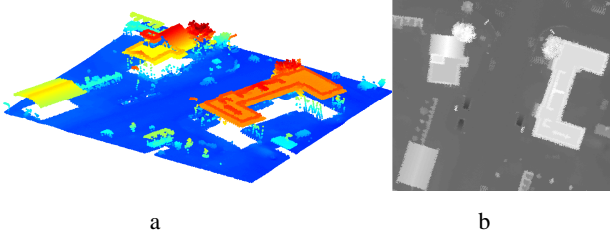


Figure 1. Point clouds measured with TopoSys® Laser scanner a) colored by height, b) raster image based on point clouds with interpolated values.

An example of data received by a terrestrial Laser scanner (Z+F sensor) for a dense point cloud colored by intensity is shown in Figure 2.

In contrary to the airborne data the projection of terrestrial Laser data along any direction is not very reasonable. Especially the combination of airborne (Figure 1) and terrestrial (Figure 2) Laserscanning data requires directly the analysis in the 3D data.



Figure 2. Point clouds of a Z+F sensor colored by intensity.

2.1 Calculation of the covariance matrix utilizing a 3D spherical volume cell

A 3D spherical volume cell with radius R is assigned to each point of the cloud. All points in a spherical cell will be analyzed. The 3D covariance matrix as described by Maas & Vosselman (1999) are discussed and further improved as described in Gross & Thoennessen (2006).

In a continuous domain, moments are defined by:

$$m_{ijk} = \int_V x^i y^j z^k f(x, y, z) dv, \quad (1)$$

where $i, j, k \in \mathbb{N}$, and $i + j + k$ is the order of the moments integrated over a predefined volume weighted by $f(x, y, z)$. As weighting function the mass density can be used. It reduces to a constant value if homogeneous material is assumed. Another possibility is to use the measured intensity as weighting function as discussed in earlier works. To normalize the terms they have to divide by the volume $m_{000} = \int_V f(x, y, z) dv$.

Considering only surfaces of objects all moments have to be calculated with a constant but small thickness for the volume vanishing by the normalization. After discretization of the integrand and setting $f(x, y, z) = 1 \forall$ points the integral is approximated by a sum. The mean values $\bar{x}, \bar{y}, \bar{z}$ and the moments of the second order $i + j + k = 2$ have been calculated.

The normalized and dimensionless moments of second order for discrete points are given by

$$\tilde{m}_{ijk} = \frac{\sum_{l=1}^N (x_l - \bar{x})^i (y_l - \bar{y})^j (z_l - \bar{z})^k}{R^{i+j+k} N}. \quad (2)$$

Neither the number of points nor the chosen physical unit for the coordinates, the radius and the weighting factor influences the values of the covariance matrix.

For each point of the whole data set a symmetrical covariance matrix is calculated by

$$M = \begin{pmatrix} \tilde{m}_{200} & \tilde{m}_{110} & \tilde{m}_{101} \\ \tilde{m}_{110} & \tilde{m}_{020} & \tilde{m}_{011} \\ \tilde{m}_{101} & \tilde{m}_{011} & \tilde{m}_{002} \end{pmatrix}. \quad (3)$$

The calculation of the eigenvalues λ_i and eigenvectors \bar{e}_i with $i=1,2,3$ delivers additional features for each point. The eigenvalues are invariant concerning translation, rotation, and scaling.

2.2 Point distribution in 3D space

In this section the influence of the measurement and the related point distribution on the investigated structures is described.

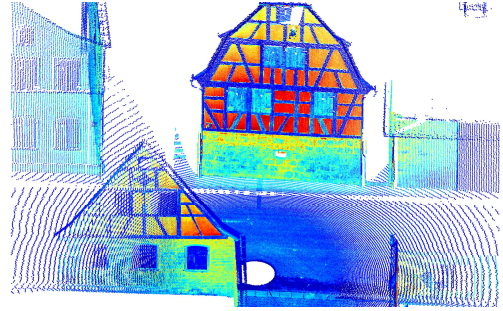


Figure 3. Illustration of a point cloud captured by a terrestrial Laser scanner with typical scan pattern (color indicates the reflected intensity).

Figure 3 shows as an example for the point distribution derived by a terrestrial Laser scanner (Zoller+Fröhlich). The point density depends on the distance of the object to the sensor and also on the incidence angle between laser beam and normal vector onto the object surface. For the airborne Laser scanner (TopoSys®) mounted on an aircraft the point density can be much higher in flight direction than perpendicular to the flight direction. In both cases there is no uniform distribution of the measured points.

The investigations show that an inhomogeneous distribution does not influence the eigenvalues essentially as long as the radius of the neighbourhood is large enough. This means points inside a plane are characterized as plane points if the neighbourhood encloses at least five points in all directions and the rate of the point distances for any two different directions is smaller than 5:1.

2.3 Analytical eigenvalues for object structures

For specific object structures analytical eigenvalues can be determined. Table 1 show some typical object structures with their corresponding eigenvalues, where all values are determined by utilizing all required integrations of formula (1).

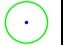
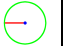
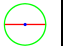
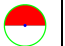
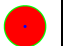

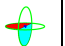


Eigenvalues		λ_1	λ_2	λ_3
	Isolated point	0	0	0
	End of a line	$\frac{1}{12}$	0	0
	Line	$\frac{1}{3}$	0	0
	Half plane	$\frac{1}{4}$	$\frac{1}{4}\left(1 - \frac{64}{9\pi^2}\right) = 0.0$	0
	Plane	$\frac{1}{4}$	$\frac{1}{4}$	0
	Quarter plane	$\frac{1}{4}\left(1 - \frac{2}{\pi}\right) = 0.09$	$\frac{1}{4} + \frac{1}{2\pi} - \frac{32}{9\pi^2} = 0$	0
	Two planes	$\frac{1}{4}$	$\frac{1}{8}$	$\frac{1}{8} - \frac{8}{9\pi^2} = 0.03$
	Three planes	$\frac{1}{6}\left(1 - \frac{1}{\pi}\right) = 0.11$	$\frac{1}{6}\left(1 - \frac{1}{\pi}\right) = 0.11$	$\frac{1}{6}\left(\frac{1}{\pi} + \frac{2}{3\pi}\right) - \frac{2^2}{3^2\pi^2} = 0.03$
	Two planes 30°	0.25	0.1875	0.01747

Table 1. Eigenvalues for some selected object structures.

For all possible values of the roof slope the eigenvalues are drawn in Figure 4. The greatest eigenvalue is 0.25 and constant. The second eigenvalue starts from 0.125 and increases with increasing slope until 0.25. The smallest eigenvalue decreases from 0.03 to zero. For a slope of 30° the eigenvalues reaches the mean values for a flat roof and a plane. Therefore an own class for this structure is defined.

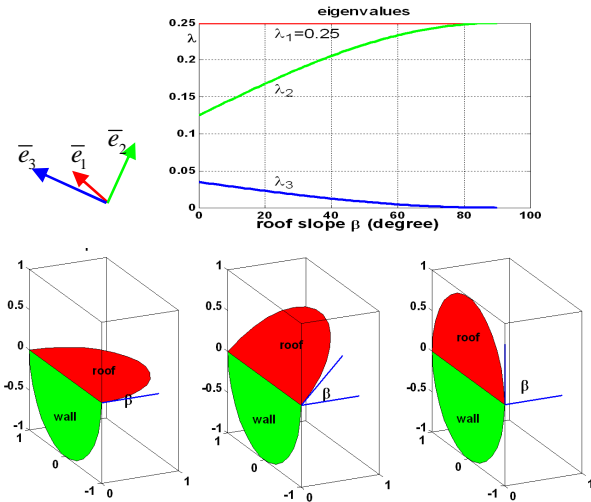


Figure 4. Eigenvalues of the eave points for different roof slopes (0°, 30°, and 90°); the colored arrows visualize the direction of the eigenvectors.

3. MONTE CARLO SIMULATION

The analytical calculated values in Table 1 do not correspond to the statistical averages, which can be expected for the relevant structures of real data. Usually, for an example, the smallest eigenvalue of points belonging to a plane do not converge to $\lambda_3 = 0$. Already very small deviations of points from a flat surface yield to $\lambda_3 > 0$. Therefore for all the structures in Table 1 inside a spherical neighbourhood with radius R points

with the different distances, normalized by the radius of the sphere $dx/R \in \{0.03, 0.1, 0.2, 0.3, 0.4\}$ are generated. Each coordinate of the position of the points is modified by a Gaussian distributed noise with the normalized standard deviation $\sigma/R \in \{0.0, 0.01, 0.02, 0.03, 0.04\}$.

For each parameter combination and structure 1000 point clouds have been generated by random 3D points. The mean value and the standard deviation of every 3 eigenvalues were determined. The histograms of one test set for each structure are drawn in Figure 5. The distribution of the eigenvalues seems to be Gaussian with center near by the analytical values.

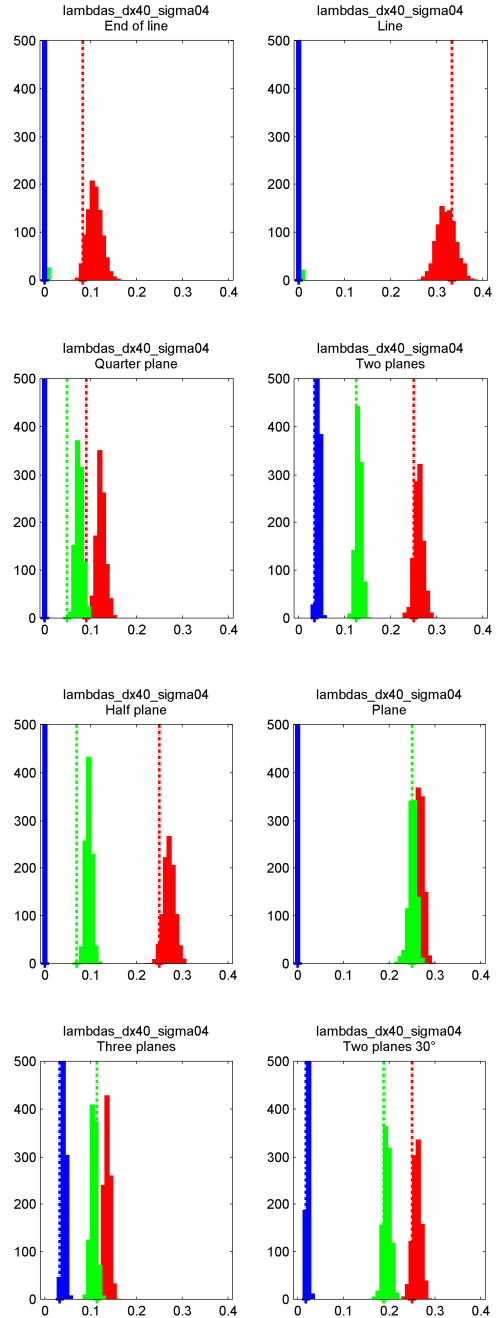


Figure 5. Histograms of the eigenvalues and comparison with the analytical values (dashed lines) for $dx = 0.4R$ and $\sigma = 0.04R$ for all structures (red: first, green: second, blue: third eigenvalue).

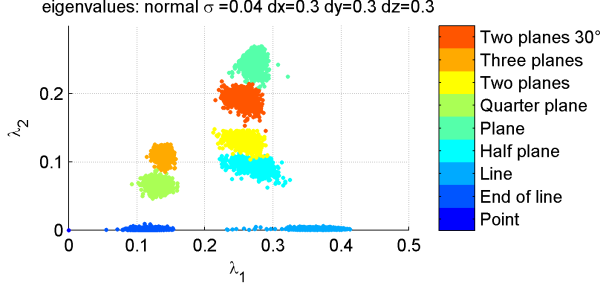


Figure 6. Eigenvalue point cloud projection along the axis of the smallest eigenvalue.

In the next steps the 3 eigenvalues are considered as a point of a 3D space. For a small standard deviation σ the point cloud of eigenvalues results in a small accumulation of points. If σ is increasing the clusters are extending and nearby clusters may overlap. Figure 6 shows the 2D-projection along the axis of the eigenvalue λ_3 . Projections along the two other eigenvalues demonstrate the separability of the cluster for each structure.

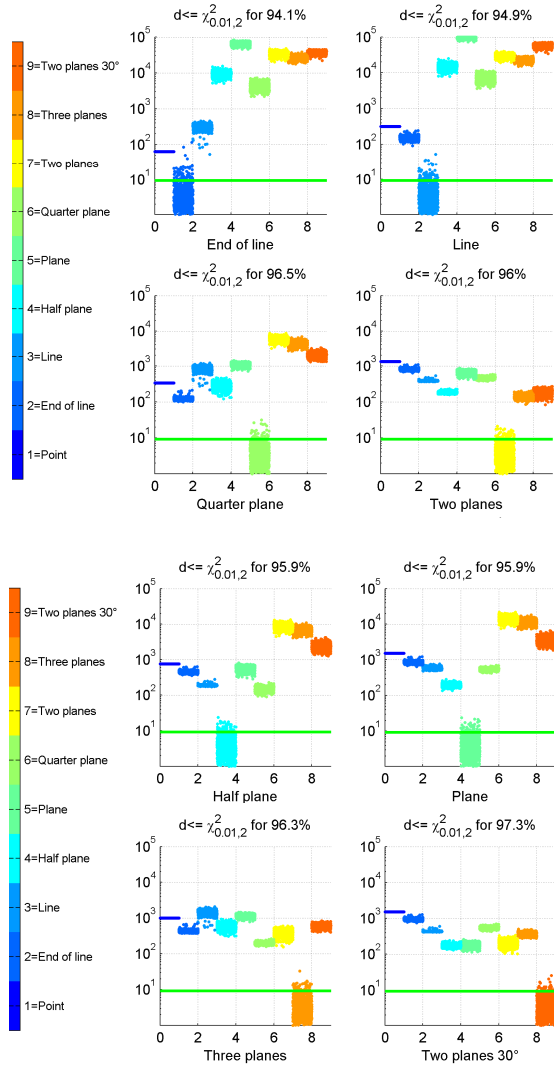


Figure 7. Distances of the eigenvalue points to all classes.

The eigenvalues of the points for each structure define a training record from which the three mean values $\bar{\lambda}_S = 1/N \sum_{p \in S} \lambda_p$ as well as the associated eigenvalue-covariance-

matrix $C_S = \sum_{p \in S} (\lambda_p - \bar{\lambda})(\lambda_p - \bar{\lambda})^T$ can be calculated, where N is the number of eigenvalue-points of the structure. The distance of any test point λ of the eigenvalue space is determined by using the Mahalanobis-distance $d(\lambda, S) = (\lambda - \bar{\lambda}_S)^T C_S^{-1} (\lambda - \bar{\lambda}_S)$. This measure gives a distance for any test eigenvalue-point to the different structures. These eight distances of every point against their own and all other structures (except for isolated point) are listed in the Figure 7. The points of a structure are plotted and colored in accordance to their membership S and drawn in the interval $[S-1, S]$ (horizontal axis). The vertical axis represents the logarithm of the distance of each eigenvalue point to each structure. In the 1st picture the distances between the eigenvectors of all test records of all structures against the structure "End of line" are drawn. The remaining pictures show the respective distance of all test points to the other structures. The green line mark the value of the Chi-square tests $\chi^2_{0.01,2}$. The percentage number of points of each structure with a smaller distance has been indicated. With increasing noise the distance of a point of a structure to a different structure decreases. Therefore false classification increases.

Figure 8 shows the mean value and the standard deviation of the eigenvalues of the training set for a plane dependent on the point density and the noise. The mean values approximate the analytical eigenvalues with a very small standard deviation.

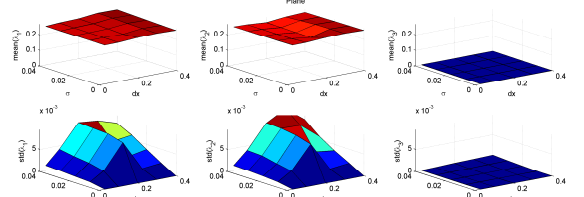


Figure 8. Mean value and standard deviation of the three eigenvalues of the training set for a plane.

A comparison between the mean value of the eigenvalues of the training set for a plane and the analytical values is shown in Figure 9. The differences depend on the point density and the noise. A high point density delivers nearly the analytical eigenvalues. The non monotonic behaviour of the curve for λ_2 may be caused by the approximation of a plane by nearly equidistant points (discretization effects). The mean value of the third eigenvalues is positive but very small.

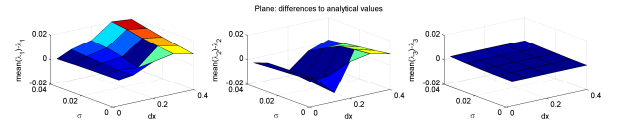


Figure 9. Differences between the mean value of the eigenvalues of the training set for a plane and the analytical values.

For the same points the Euclidean distances in the eigenvalue space against the analytical eigenvalues were calculated. Within the tested mean point intervals and the investigated noise all the points were assigned to the correct structure. Based on this investigation the classification of elevation points can be realized by nearest neighbour classification in the eigenvalue space of the structures of Table 1. This is possible as far the noise is lower than 4% of the radius of the neighbourhood environment.

4. NEAREST NEIGHBOUR CLASSIFICATION OF 3D POINTS

After calculating the covariance matrix for each point in the data set by considering the local environment defined by a sphere additional features for each point are derived. These features are the centre of gravity, the geometrical distance between centre of gravity to the point, the eigenvectors, the eigenvalues and the number of points inside the sphere. The same features can be used to determinate the object characteristics.

Table 1 shows the eigenvalues of the covariance matrix of some special point configurations. The first six rows present 2D and the last three rows 3D object structures. The eigenvalues for the typical object structures are calculated analytically. For an ideal line two eigenvalues are zero and one of it is greater than zero. If test points inside a plane are of interest their eigenvalues have to be compared with the analytical eigenvalues $\lambda_1 = \lambda_2 = 0.25 \wedge \lambda_3 = 0$ for a correct plane.

The eigenvalues in Table 1 are considered as reference points in the 3D eigenvalue space for each structure. The classification of any test point by the nearest neighbour method was performed, were all distances were measured in the eigenvalue space.

For the following steps we define the dimensionality $\dim(S)$ for each structure, which means the dimension of all points belonging to the same structure of a contiguous object. The dimensionalities for each structure are given in Table 2. Corner like points have the dimensionality 0, edge like points 1 and plane like points 2.

Structure	Dimensionality
Isolated point	0
End of a line	0
Line	1
Half plane	1
Plane	2
Quarter plane	0
Two planes	1
Three planes	0
Two planes 30°	1

Table 2. Dimensionality for each structure.

By utilizing the empirically derived weighting factors $w(S) = 1/(1 + \dim(S))$ for the distance $d(S)$ between the test point and the analytically calculated eigenvalues of structure S the classification result was refined. This weighting of the distances between test and reference points introduces non-planar separation surfaces defined by $d(S_i)w(S_i) = d(S_j)w(S_j)$ between two structures. Ignoring the influence of all other structures, the separation surface between the structures i and j is given by the constant ratio of both distances $d(S_i)/d(S_j) = w(S_j)/w(S_i) = w_{ji}$. For $w_{ji} = 1$ we get the intermediate plane between both structures as separation surface. For $w_{ji} \neq 1$ the separation is described by a sphere. Radius and centre point depend only on w_{ji} and the distance between the two structures in the 3D eigenvalue space.

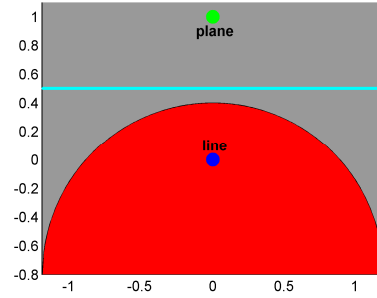


Figure 10. Equipotential surface between line and plane in the eigenvalue space.

As an example Figure 10 illustrates the situation between the structures *line* and *plane* with weighted distances. All test points with eigenvalues inside the red region are classified as line points meanwhile all points in the grey region are classified as points belonging to a plane. Without weighting the cyan marked horizontal line (hyper plane) separates the two classes.

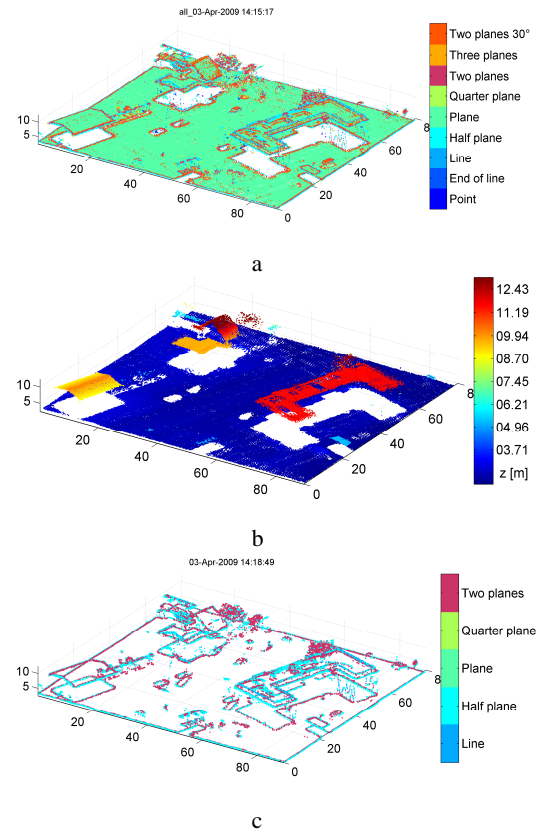


Figure 11. Classified object points. a) All points colored by their classification, b) Points identified as plane points (colored by their height), c) Points with one high and two small eigenvalues representing edges of objects.

By utilizing the weighted distance calculation during the classification procedure for all points the derived results are shown in Figure 11a. Figure 11b shows all points with eigenvalues fulfilling the criteria for planes. The color indicates the object height. In Figure 11c only the edge points are depicted corresponding to Table 1 rows 3, 4, and 7.

For the introduced classification further results are shown for comparison purposes of a more complex building. The results are depicted in Figure 12 with an oblique view to demonstrate the geometrical relation of the 3D points.

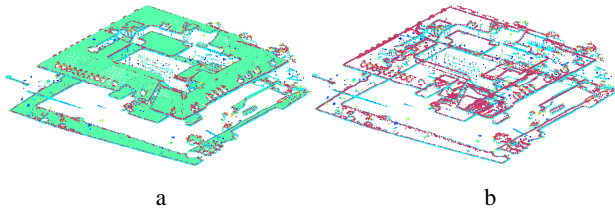


Figure 12. Classification result of a laser point cloud for a complex urban building. a) with all points, b) without points inside a plane.

5. LINE GENERATION

All points marked as edge point may belong to a line. These points are assembled to lines by a grouping process (Gross & Thoennessen, 2006). Therefore the greatest eigenvalue and its eigenvector are considered. Consecutive points with a similar eigenvector, lying inside a small cylinder are grouped together and approximated by a line.

The procedure starts with any arbitrary point of the point cloud classified as edge-like point (*line, halfplane, two_planes*). This trigger point is compared with all points which have nearly the same or opposite eigenvector of the largest eigenvalue. Furthermore only points with very small distance to the straight line defined by the trigger point and its first eigenvector are included in the next consideration. Finally it is focused on the first two gaps starting from the trigger point going along the first eigenvector and also its opposite direction. Only points inside these gaps and fulfilling all those conditions are selected and used to determine a regression line and its endpoints.

The same procedure is repeated for all points not assigned to a line until each point belongs to a line or can not generate an acceptable line.

Figure 13 shows the results of the line generation for the data set shown in figure 1. The color indicates the length of the lines. The eaves as well as the ground plan of the buildings are approximated by lines. For the detection of the ridge of the saddle roof a readjustment of the thresholds for the eigenvalues might be recommended to improve the results especially for roofs with small inclination.

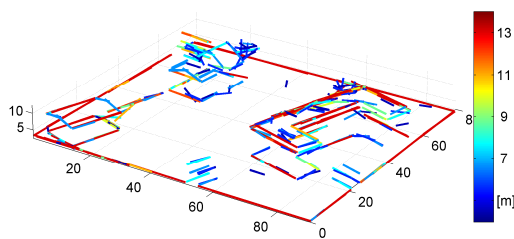


Figure 13. Lines generated by using the classified laser elevation points.

6. CONCLUSION AND OUTLOOK

For exploiting Laser scanning data the processing of the original 3D point clouds is proposed. Additional features for each point of the cloud can be calculated from the covariance matrix including all neighbour points. The neighbourhood can be investigated by considering a sphere. The quality of the resulting eigenvalues and the eigenvectors of the matrix strongly depend on the spatial resolution and the number of points inside the sphere. The new features are invariant with respect to position, rotation and scale.

The additional features are appropriate for classification of the points as edge, corner, plane or tree points. For some typical situations analytically determined eigenvalues are opposed to calculated eigenvalues of real data for comparison. The greatest eigenvalue can be used for filtering edge like points.

The described method for generation of lines combines consecutive points with the same eigenvector inside a small cylinder without any gap. The presented results are promising.

Further investigations are planned concerning the fusion of the data on basis of the point clouds and/or on a higher level of lines. Especially the construction of planes assembling plane like points should be investigated in future.

REFERENCES

- Baillard, C., Schmid, C., Zisserman, A., Fitzgibbon, A., 1999. Automatic line matching and 3D reconstruction from multiple views. In: ISPRS Conference on Automatic Extraction of GIS Objects from Digital Imagery 32, pp. 69-80.
- Brenner, C., Haala, N., Fritsch, D., 2001. Towards fully automated 3D city model generation. In: Baltsavias, E., Gruen, A., van Gool, L., (Eds), Proc. 3rd Int. Workshop on Automatic Extraction of Man-Made Objects from Aerial and Space Images, pp. 47-57.
- Fraser, C.S., Baltsavias, E., Gruen, A., 2002. Processing of IKONOS Imagery for Submetre 3D Positioning and Building Extraction. ISPRS Journal of Photogrammetry and Remote Sensing 56 (3), pp. 177-194.
- Geibel, R., Stilla, U., 2000. Segmentation of Laseraltimeter data for building reconstruction: Comparison of different procedures. International Archives of Photogrammetry and Remote Sensing 33 (Part B3), pp. 326-334.
- Gross, H., Thoennessen, U., 2005. 3D Modeling of Urban Structures. Joint Workshop of ISPRS/DAGM Object Extraction for 3D City Models, Road Databases, and Traffic Monitoring CMRT05, International Archives of Photogrammetry and Remote Sensing 36 (Part 3/W24), pp. 137-142.
- Gross, H., Thoennessen, U., 2006. Extraction of Lines from Laser Point Clouds. In: Förstner, W., Steffen, R., (Eds) Symposium of ISPRS Commission III: Photogrammetric Computer Vision PCV06. International Archives of Photogrammetry, Remote Sensing and Spatial Information Sciences 36 (Part 3), pp. 86-91.
- Jutzi, B., Neulist, J., Stilla, U., (2005) High-Resolution waveform acquisition and analysis for pulsed laser. In: Heipke, C., Jacobsen, K., Gerke, M. (Eds.) High-resolution earth imaging for geospatial information. International Archives of Photogrammetry and Remote Sensing 36 (Part 1 W3) (on CD).
- Kirchhof, M., Jutzi, B., Stilla, U., (2008) Iterative processing of laser scanning data by full waveform analysis in close neighborhood. In: Lichti, D., Pfeifer, N., Maas, H.-G., (Eds.) ISPRS Journal of Photogrammetry & Remote Sensing 63 (1): pp. 99-114. [doi:10.1016/j.isprsjprs.2007.08.006]
- Maas, H.-G., Vosselman, G., 1999. Two algorithms for extracting building models from raw Laser altimetry data. ISPRS Journal of Photogrammetry & Remote Sensing 54 (2-3), pp. 153-163.
- Pollefeys, M., 1999. Self-Calibration and Metric 3D-Reconstruction from Uncalibrated Image Sequences, PhD-Thesis, K. U. Leuven.
- Shan, J., Toth, C.K., (Eds.) 2008. Topographic Laser Ranging and Scanning: Principles and Processing. Boca Raton, FL: Taylor & Francis.
- Vosselman, G., Gorte, B., Sithole, G., Rabbani, T., 2004. Recognizing structure in Laser scanner point clouds. Int. Archives of Photogrammetry, Remote Sensing and Spatial Information Sciences 46 (Part 8/W2), pp. 33-38.